JOURNAL OF GEOPHYSICAL RESEARCH, VOL. 112, D14301, doi:10.1029/2006JD008085, 2007

Click Here for Full Article

A comparison of CMAQ-based aerosol properties with IMPROVE, MODIS, and AERONET data

Biswadev Roy,[1] Rohit Mathur,[1,2] Alice B. Gilliland,[1,2] and Steven C. Howard[1,2]

Received 28 September 2006; revised 12 January 2007; accepted 28 February 2007; published 19 July 2007.

[1] Evaluation of concentrations predicted by air quality models is needed to ensure that model results are compatible with observations. In this study aerosol properties derived from the Community Multiscale Air Quality (CMAQ) model-simulated aerosol mass concentrations are compared with routine data from NASA satellite-borne Moderate Resolution Imaging Spectroradiometer (MODIS) sensor aboard the Sun-synchronous Terra satellite, NASA's ground-based Aerosol Robotic Network (AERONET), and the ground-based Interagency Monitoring of Protected Visual Environment (IMPROVE) network. The motivation for this analysis is to determine how best to use these parameters in evaluating model-predicted $PM_{2.5}$ concentrations. CMAQ surface extinction estimates due to scattering at 550 nm wavelength are compared with the IMPROVE nephelometer data obtained from 25 sites within the United States. It is found that model-predicted surface extinctions bear high correlations with nephelometer measured data. Sulfate fractional aerosol optical depth (AOD) is found to dominate in the northeastern part of the United States; hence ground-based measurement of sulfate concentrations have been compared with time series of columnar AOD as observed by the MODIS instrument and also with the CMAQ-predicted tropospheric column values obtained during the June–August period of 2001. CMAQ surface extinctions are found to be relatively higher than the IMPROVE nephelometer observations; however, there is a good agreement between CMAQ AOD trends and AERONET and MODIS data, obtained at the seven AERONET sites located in the eastern United States. CMAQ is also found to capture the day-to-day variability in the spatial AOD patterns. Monthly average satellite AOD estimates are found to be higher than the AOD data obtained using the CMAQ-predicted aerosol concentrations. Seasonal variation of satellite-measured aerosol intensive property "Angstrom exponent" (a gross indicator of the aerosol size distribution) is presented for four selected sites: one each in the eastern and central parts, and two in the western part of the continental United States. Variability of Angstrom exponent at these four selected sites is analyzed in conjunction with the variation of summertime AOD (observed and modeled), mass concentration (observed and modeled) and modeled SO_4 average concentrations during the summer (June–August) period of the year 2001. Annual time series of Angstrom exponent data at the four selected sites show a large east-west variation.

Citation: Roy, B., R. Mathur, A. B. Gilliland, and S. C. Howard (2007), A comparison of CMAQ-based aerosol properties with IMPROVE, MODIS, and AERONET data, *J. Geophys. Res.*, *112*, D14301, doi:10.1029/2006JD008085.

1. Introduction

[2] Aerosol particles can affect climate directly by the interaction with incoming short-wave solar and outgoing long-wave terrestrial radiation. Aerosols also exhibit direct radiative forcing and indirect effects on clouds and precipitation [*Kaufman et al.*, 1997; *Penner et al.*, 1994]. These, in turn greatly influence the characteristics of the tropospheric boundary layer and photochemical reactions. The monthly average variation in aerosol type as a function of space and time depends on the proximity and temporal variation of sources and the chemical reactivity of aerosol precursors under different meteorological conditions. Aerosols may include many different types of primary and secondary species, namely sulfates (SO_4), ammonium (NH_4), nitrates (NO_3), organic carbon (OC) species, and black or elemental carbon (BC) from different types of sources.

[3] The U.S. Environmental Protection Agency (USEPA) regulates ambient particulate matter as criteria pollutants in an aggregate sense with total $PM_{2.5}$ (particles having an

[1] Atmospheric Modeling Division, National Exposure Research Laboratory, U.S. Environmental Protection Agency, Research Triangle Park, North Carolina, USA.
[2] Atmospheric Sciences Modeling Division, Air Resources Laboratory, NOAA, Research Triangle Park, North Carolina, USA.

Copyright 2007 by the American Geophysical Union.
0148-0227/07/2006JD008085$09.00

aerodynamic diameter $\leq$ 2.5 μm) standards with limits on the 24-hour average and annual average concentrations. Air quality models are being used in the air quality decision-making process in order to determine the levels of emission reductions for individual aerosol species of concern necessary to comply with the standards. Since models are used in the regulatory process, it is essential that their performance be evaluated thoroughly. Atmospheric chemical processes are responsible for sulfate peaks in summer months and nitrate peaks in winter throughout much of the United States. Sulfates are primarily a product of sulfur-dioxide (SO_2) emissions and photochemical reactions in the atmosphere. Highest sulfate mass concentrations are found in the central eastern United States, whereas the nitrate concentrations are found to be high in southern part of California [*Malm et al.*, 2004] and in the northern Midwest regions (based on recent observations from new sites in the mid-western United States). East of the Rocky Mountains, nonurban regional $PM_{2.5}$ is predominantly composed of SO_4 and NO_3 aerosols. Several monitoring networks provide surface-level observations of $PM_{2.5}$ and $PM_{2.5}$ species components, but they do not provide full spatial coverage for a meaningful evaluation of the model predictions. Previous studies have demonstrated relatively high correlations between remotely sensed aerosol optical depth (AOD) values and surface level observed $PM_{2.5}$ concentrations in the range 0.6–0.8 [e.g., *Liu et al.*, 2004; *Al-Saadi et al.*, 2005]. A strong relationship between surface $PM_{2.5}$ and AOD suggests that AOD could be an useful additional metric for evaluating an air quality model and its ability to predict atmospheric aerosol loading. Therefore the purpose of this study is to assess whether satellite-derived AOD data provide supplementary information for the evaluation of $PM_{2.5}$ model predictions.

[4] The air quality model and observational data sets used in this study are described in section 2. In order to verify the usefulness of the satellite-measured AOD as an additional property in conjunction with surface-based $PM_{2.5}$ observations we present in this paper comparisons of the particle scattering extinctions from Interagency Monitoring of Protected Visual Environment (IMPROVE) nephelometer sites with those obtained from Community Multiscale Air Quality (CMAQ). Results of the direct comparison with nephelometer data are presented in section 3. Chemical apportionment of the AOD column for the northeastern (NE) United States is done using modeled fractional AOD data for sulfate, ammonium, nitrate, elemental and organic carbon, and studies on the time variation of sulfate at few selected Aerosol Robotic Network (AERONET) sites in the NE sector are mentioned in section 4. Since the Angstrom exponent is an indicator of particle size variability, we also compare observed Angstrom exponents across the United States to consider the spatial difference in gross particle size distribution over the eastern United States.

2. Methodology

2.1. CMAQ Model Description

[5] The 3-D distribution of $PM_{2.5}$ and its chemical constituents over the continental United States was generated for the year 2001 using the CMAQ model version 4.5 [*Byun and Schere*, 2006; *Byun and Ching*, 1999]. The CMAQ model simulations were performed using the Carbon Bond IV chemical mechanism [*Gery et al.*, 1989]. The CMAQ modeling domains covered the contiguous United States and portions of Canada and northern Mexico with horizontal grid resolution of 36km x 36km. The CMAQ aerosol predictions are based on a modal aerosol model [*Binkowski and Roselle*, 2003] and the ISORROPIA (meaning "equilibrium" in Greek) thermodynamic equilibrium model [*Nenes et al.*, 1998]. Chemical lateral boundary conditions for CMAQ were based on a global-scale chemical transport model, the Goddard Earth Observing System-Chemistry (GEOS-CHEM) [*Bey et al.*, 2001].

[6] The Penn State/NCAR Mesoscale Model (MM5) version 3.6.1 [*Grell et al.*, 1994] was used to develop the meteorological data fields for CMAQ. The MM5 model was run in reinitialized 5.5-day segments (first 12 hours of each run is not used by the CMAQ). Model simulations were performed with the physics options: the Pleim-Xiu land surface model [*Xiu and Pleim*, 2001; *Pleim and Xiu*, 2003], the rapid radiative transfer model (RRTM) long-wave radiation [*Mlawer et al.*, 1997], *Dudhia*'s [1989] short-wave radiation scheme, the Kain-Fritcsh subgrid-scale cumulus parameterization scheme [*Kain*, 2004], and the Reisner 2 microphysics scheme [*Reisner et al.*, 1998]. Simulations were performed using analysis nudging for the winds, temperature, and moisture and using the Asymmetric convective model for planetary boundary layer (PBL) model [*Pleim and Chang*, 1992]. All other details about the meteorological simulations performed using the MM5 version 3.6.1 are given by *Gilliam et al.* [2006]. Both the MM5 and CMAQ simulations were conducted at 36 km $\times$ 36 km horizontal dimensions for the entire year of 2001. The model-ready meteorology fields were developed using the Meteorology-Chemistry Interface Processor (MCIP) version 2.2, and the MM5 vertical layer structure was collapsed from 34 layers to 14 sigma layers between the surface and100 mbar, with the first layer being 36 m thick.

[7] Mobile source emissions were generated using the MOBILE6 model [*U.S. Environmental Protection Agency*, 2003] and the BEIS3.12 model was used for estimating biogenic emissions (available at http://www.epa.gov/asmdnerl/biogen.html). MOBILE6 is a model that calculates emissions of hydrocarbons (HC), oxides of nitrogen (NOx) and carbon monoxide (CO) from passenger cars, motorcycles, light- and heavy-duty trucks. MOBILE is based on emissions testing of tens of thousands of vehicles. The model accounts for the emission impacts of factors such as changes in vehicle emission standards, changes in vehicle populations and activity, and variation in local conditions such as temperature, humidity and fuel quality.

[8] The emission inventory for other sources was based on the USEPA National Emissions Inventory (NEI) for 2001. The seasonality of ammonia emissions, an important consideration for prediction of inorganic aerosols was estimated on the basis of current best estimates [*Gilliland et al.*, 2006; *Pinder et al.*, 2004]. In the current algorithm climatological dust emission estimates are used as opposed to using an explicit dust emissions model which responds to local meteorological factors.

Table 1. R and RMSE From the Summer 2001 (June–August) CMAQ v4.5 Simulation[a]

	SO_4 (R, RMSE)	NH_4 (R, RMSE)	NO_3 (R, RMSE)	OC (R, RMSE)	BC (R, RMSE)	Total Carbon (R, RMSE)
IMPROVE	0.86, 2.02	N/A	0.32, 0.49	0.22, 2.02	0.32, 0.36	0.23, 2.34
CASTNET	0.89, 2.32	0.82, 0.80	0.20, 0.58	N/A	N/A	N/A
STN	0.83, 2.75	0.71, 1.09	0.27, 2.02	N/A	N/A	0.43, 2.52

[a]Unit is μg m^{-3}. Model results are compared to data from the Interagency Monitoring of Protected Visual Environments (IMPROVE) network, the Clean Air Status and Trends Network (CASTNET), and the Speciated Trends Network (STN). This table is based on the report by *Appel et al.* [2005].

2.2. CMAQ-Derived AOD Estimates

[9] The intensity of light is attenuated in the atmosphere mostly by aerosol scattering. The extinction coefficient (σ_e) is the fraction of intensity lost from a collimated beam per unit atmosphere layer thickness; the commonly used units are km^{-1} or m^{-1}. The AOD is obtained by integrating the extinction coefficient at a given wavelength from surface to the top-of-atmosphere (TOA). Extinction (σ_e), which is a function of wavelength (λ), is the sum of attenuation by scattering (σ_s) and absorption (σ_a):

$$\sigma_e(\lambda) = \sigma_s(\lambda) + \sigma_a(\lambda) \tag{1}$$

The scattering and absorptive coefficients can be written as:

$$\begin{aligned} \sigma_s(\lambda) &= b_{sp}(\lambda) + b_{sg}(\lambda) \\ \sigma_a(\lambda) &= b_{ap}(\lambda) + b_{ag}(\lambda) \end{aligned} \tag{2}$$

where b_{sp}, b_{sg}, b_{ap}, and b_{ag} are the extinctions due to particle scattering, gaseous scattering, particle absorption, and gaseous absorption, respectively. The contribution of gaseous component (b_{sg}) in (2) is due to Rayleigh (natural class) scattering mostly due to oxygen and nitrogen molecules, and we will neglect this term in our analysis. Similarly, we also neglect the contribution due to gaseous absorption (b_{ag}) term in equation (2) because of its insignificant magnitude compared with fine particulate matter scattering. With these assumptions we estimate the model-predicted AOD due to particulate scattering and absorption by summing the product of total extinction and layer thicknesses (ΔZ_i):

$$AOD_{model} = \sum_{i=1}^{N} \left(\sigma_{sp} + \sigma_{ap}\right)_i \Delta Z_i \tag{3}$$

The method used here for estimating the extinctions due to scattering and absorption in equation (3) is a semiempirical mass extinction method described by *Malm et al.* [1994] and *Binkowski and Roselle* [2003]. This method is termed as the "reconstructed mass-extinction (RM) method." Hereinafter we will use "RM" for denoting this particular semiempirical approach for extinction calculation,

$$\begin{aligned} b_{sp} &= (0.003) f_t(RH)\left[NH_4^+ + SO_4^- + NO_3^-\right] \\ &\quad + 0.004 * [OM] + (0.001)[FS] + (0.0006)[CM] \\ b_{ap} &= (0.01)[LAC] \end{aligned} \tag{4}$$

where the brackets in the above equation indicate mass concentration in mg m^{-3}. Abbreviations OM, FS, CM, and LAC represent organic mass, fine soil, coarse mass, and light-absorbing carbon, respectively. The fine soil (FS) part of the specific scattering coefficient is derived by adding the accumulation and Aitken mode unspecified anthropogenic mass and the soil mass which is obtained from the CMAQ model runs. LAC is derived using the black (elemental) carbon concentration. The specific scattering coefficient of 0.003, 0.004, 0.001, 0.0006 and 0.01 used respectively in (4) have units m^2 mg^{-1}, and are based on assuming a lognormal particle size distribution [*Malm et al.*, 1994]. The mass concentration for each of these species is directly obtained from the CMAQ simulation described in the previous section. The relative humidity based aerosol growth factor f_t (RH) is based on a look-up table [*Malm et al.*, 1994]. Using the modeled pressure level, water vapor mixing ratio and temperature, we compute the vapor pressure and RH. This RH value is then used to locate the exact humidity growth factor from the look up table [*Binkowski and Roselle*, 2003; *Malm et al.*, 1994]. CMAQ v4.5 results from this 2001 simulation have been extensively compared with surface network data as part of the model release evaluation [*Appel et al.*, 2005]. Table 1 shows the correlation coefficient (R) and the root-mean-square error (RMSE) from that analysis where model simulated data were compared with data obtained from three different surface networks.

2.3. Terra/MODIS-Derived Land-Corrected Aerosol Optical Depth Product

[10] Since aerosols in the atmosphere have a short life span, spaceborne observations over large regions that capture their spatial variability could potentially be used more effectively for monitoring aerosol loading than using expensive and sparse ground based aerosol monitoring data. The MODIS sensor aboard the Earth Observing System (EOS) Terra spacecraft is utilized in this study. The MODIS AOD retrieval algorithm uses the satellite measured radiance/reflectance through the use of a finite look-up table (LUT) as mentioned by *Kaufman and Tanré* [1998]. Derivation of the LUT includes corrections of multiple scattering. Atmospheric path radiance is a function of the total optical depth (path-extinction) which includes both aerosol scattering/absorption (Mie approximation) and molecular scattering (Rayleigh theory). The total radiance/reflectance observed by the satellite is the sum of the atmospheric path radiance and the transmitted part of the surface albedo. Uncertainties due to the surface are minimized; aerosol retrievals are performed over "dark targets" so that the signal has minimum noise due to other surface sources [*Kaufman et al.*, 1997]. Over the land, the surface reflectances are unknown; hence it has to be inferred by other means [*Kaufman et al.*, 1997]. Over many vegetated areas of the world, the surface reflectance in visible (VIS) wave-

lengths is proportional to that in the solar infrared (IR) wavelengths. Assuming that aerosol is transparent in the IR wavelengths (aerosol size smaller than λ - Mie theory), the MODIS observed reflectance is essentially the surface reflectance, thus allowing inference of the surface reflectance in visible wavelengths. The difference between observations and surface reflectance is due to path radiance, which determines aerosol properties. There are fixed, and minimal choices for aerosol model properties (e.g., single scattering albedo (SSA), and phase function), and the variance in assumed VIS/IR surface reflectance ratios [*Kaufman et al.*, 2002] as mentioned by *Levy et al.* [2005]. The ratios of the single scattering path radiances (0.47 μm and at 0.66 μm) and the AOD at 0.47 μm are used to generate a decision tree to decide which kind of aerosol predominates in a given grid box and then an aerosol model is selected that best describes the aerosol size distribution in that box, assigns refractive index and single scattering albedo, and also describes the nonsphericity on the phase function. These models are based on in situ column aerosol size distribution measurements taken using ground instruments at different places around the world. The chosen model is used to generate a LUT. Satellite measured reflectance is inverted into AOD, and mass concentration. An interpolation is then performed to obtain optical depth at 0.55 μm. Daily optical depth and mass concentration are stored in a 10 $\times$ 10 pixels resolution (1000 m nadir resolution).

[11] Since Terra is a Sun-synchronous satellite; there are two possible observations for the same region every day, one during the daylight period and one during the night. AOD samples are obtained for the daytime overpasses only because there is no surface reflectance during nighttime. The MODIS level 2 (swath) validated product used in this study is named as MOD04_L2. Each product file covers a 5-min time interval. The output grid is 135 pixels in width by 203 pixels in length. The MODIS optical depth is obtained from the MOD04_L2 science data set number 23, which contains land-corrected AOD product at 550 nm [*Remer et al.*, 2005]. For the comparisons presented here, the 10-km square tessellation AOD data in latitude/longitude coordinates are mapped to the CMAQ grid on a Lambert Conformal projection. If multiple MODIS observations were present in a single CMAQ grid, they were averaged in preparing daily paired data. CMAQ data are averaged for the period 1500–2000 UTC for all the grid cells since this is the period when the Terra satellite covers the continental United States. Examination of the functional dependence between the coefficient of variation and the number of MODIS observations per grid cells showed that the standard deviation of MODIS AOD observations for the CMAQ grid cell typically varies between 20% and 30% of the cell mean AOD value. Monthly means for both the model and MODIS were then computed from these data. Spatial plots of these monthly average MODIS AOD compared very well with NASA Goddard Earth Sciences Data and Information Services (GES DISC) Interactive Online Visualization and Analysis Infrastructure (GIOVANNI), thus providing confidence in our processing of the MODIS level 2 product. We have used the level 2 data for the period 1–14 June 2001 (since there are no orbital data for the period 15–30 June 2001), 1–31 July, and 1–31 August during summer period of 2001. The hourly CMAQ and AERONET AOD column data have also been averaged accordingly for producing monthly statistics of the aerosol properties.

2.4. IMPROVE Network Data

[12] The IMPROVE monitoring network measures fine and coarse aerosols in the Federal class I (rural) areas throughout the United States [*Malm et al.*, 2004]. The network collects 24-hour $PM_{2.5}$ and PM_{10} (all particles having aerodynamic diameter less than or equal to 2.5 μm, and 10 μm, respectively) samples every third day. The $PM_{2.5}$ samples are analyzed for mass, elemental composition, ions, and organic and elemental carbon. The data are sufficient for reconstruction of the major aerosol components such as ammonium sulfate and nitrate, organics, LAC and soil which account for most of the measured fine mass. Twenty-eight IMPROVE nephelometer sites in the eastern United States identified in Table 2 have been used to provide a comparison of monthly surface extinction due to particle scattering b_{sp}. The reprocessed hourly IMPROVE nephelometer (raw) data were obtained from the Visibility Information Exchange Web System (VIEWS) web site (http://vista.cira.colostate.edu/views/). Nephelometer b_{sp} values are generated by subtracting a fixed Rayleigh scattering value for each site from each scattering measurement. The extinction value represents attenuation due to particle scattering only. These data are converted from Mm^{-1} (per megameter) to km^{-1} and then compared with the corresponding surface extinctions predicted by CMAQ. The IMPROVE data were reported every third day; hence CMAQ site-month average data were averages of the data for the IMPROVE observation days only.

2.5. AERONET Data

[13] The AERONET network is composed of ground based Sun photometers (manufactured by Cimel Electronique, France) that observe the Sun and sky radiances and can be used to infer information about the aerosols including columnar AOD, are retrieved [*Holben et al.*, 1998]. Data from this network provide near real time observations of AOD, aerosol size distributions and precipitable water in diverse aerosol regimes. In this study we use data from 7 sites (Table 3) for comparing with the CMAQ grid cell averaged tropospheric AOD column. We have used the intermediate level 1.5 real-time cloud screened data which may not have the final calibration applied. The optical depth reported by AERONET has a spectral dependence, and the Angstrom wavelength exponent is normally used to quantify the spectral dependence of AOD [*Eck et al.*, 1999]. Following *Eck et al.* [1999] as mentioned by *King and Byrne* [1976] and *Hauser et al.* [2005] we estimate the AERONET AOD at 550 nm using the formula:

$$\ln(AOD) = a_0 + a_1 \ln\lambda + a_2(\ln\lambda)^2 \quad (5)$$

Using AOD at 16 wavelengths as measured by the AERONET system we derived the second-order polynomial fit and the coefficients in equation (5) (a_0, a_1, and a_2) following *Eck et al.* [1999] and *Hauser et al.* [2005]. Using the spectral dependence captured in (5) we then estimate AOD at λ = 550 nm for comparing with the MODIS and

Table 2. Details of the 25 IMPROVE Nephelometer Sites With Location (Latitude and Longitude in Degree) and Station Elevation (in Meters Above Mean Sea Level)[a]

Site	Location	Latitude, deg	Longitude, deg	Elevation (Above Sea Level), m
ACAD1	Acadia National Park, ME^{0*}	44.37	−68.26	122
BIBE1	Big Bend National Park, TX^{0}	29.30	−103.18	1058
BLIS1	D.L. Bliss State Park, NV^{1}	38.97	−120.10	2116
COGO2	Columbia River Gorge N. Scenic, OR^{0}	45.56	−122.21	243
CORI1	Columbia River Gorge, OR^{0}	45.66	−121.00	198
CRAY1	Craycroft (Tucson urban), AZ^{1}	32.20	−110.87	809
GICL1	Gila Wilderness, NM^{0}	33.22	−108.24	1783
HANC1	Hance Camp at Grand Canyon, AZ^{0}	35.97	−111.98	2266
GRER1	Greer, CA^{1}	34.06	−109.43	2513
GRGU1	Great Gulf Wilderness, NH^{1*}	44.31	−71.22	439
GRSM1	Great Smoky Mountains National Park, NC^{0*}	35.63	−83.94	793
HUMB1	Humbolt, NV^{1}	33.98	−111.78	1586
IKBA1	Ike's Backbone, AZ^{1}	34.34	−111.68	1303
JARI1	James River Face Wilderness, VA^{0*}	37.62	−79.51	299
LOPE1	Lone Peak Wilderness, UT^{0}	40.44	−111.71	1745
LTBV1	Lake Tahoe Boulevard, NV^{1}	38.95	−119.96	1902
MACA2	Mammoth Cave National Park, KY^{0*}	37.13	−86.14	236
MILW1	Milwaukee, WI^{1}	43.00	−87.89	193
MORA1	Mount Rainier National Park, WA^{0}	46.75	−122.12	421
MOZI2	Mount Zirkel Wilderness, CO^{0}	40.53	−106.67	3224
MUSR1	Muleshoe, AZ^{1}	32.35	−110.23	1402
PHON1	Phoenix, AZ^{1}	33.50	−112.1	372
SHEN1	Shenandoah National Park, VA^{0*}	38.52	−78.23	1073
SIAN1	Sierra Ancha, AZ^{1}	34.09	−110.94	1595
LTBV2	Lake Tahoe Boulevard, NV^{1}	38.95	−119.96	1902

[a]The site name has a superscript 0 or 1 meaning if nephelometer data are from an IMPROVE site (superscript 0) or from a non-IMPROVE location (superscript 1). The site locations shown with a superscript asterisk denote the eastern United States sites used for comparing total extinctions with the model as shown in Figure 2.

CMAQ AOD. In the following sections we have provided comparison results of modeled surface extinctions and AOD data with surface based and space based observations which are averaged over monthly timescale.

3. Comparison of CMAQ Surface Extinction With Nephelometer Data

[14] The nephelometer surface extinction due to particle scattering data are converted to 1/km and then averaged for the entire month. Figure 1 presents the scatterplots between the CMAQ-derived monthly mean surface extinction value and the corresponding measured values from the 25 nephelometer sites showing the correlation (R^2) of 0.89, 0.72, and 0.82 during the months of June, July and August 2001, respectively. The hourly, daily, and monthly CMAQ to nephelometer correlation coefficients (R) for August are 0.09, 0.39, and 0.90, respectively. The harmonic mean of the CMAQ hourly series of b_{sp} taken from all the 25 IMPROVE nephelometer sites was found to be 0.012 and for the daily series it was 0.030 whereas for the monthly case it was 0.035. This signifies that there is a sharp change of mean from hourly to daily timescale whereas the mean value of the CMAQ surface extinctions change very conservatively when timescales are changed from daily to monthly scales. In Figure 2, IMPROVE nephelometer monthly mean total extinction due to particle scattering (b_{sp}) for the 7 sites that lie in the eastern U.S. domain (identified in Table 2) are plotted as colored diamonds and overlaid on the CMAQ monthly average surface extinction plots for August 2001. The difference between CMAQ and IMPROVE surface extinction values become more prominent in the NE sector of the continental United States, where the CMAQ versus IMPROVE difference is found to lie in the range -0.05 km^{-1} and 0.1 km^{-1}. The points in Figure 1 with maximum bias in CMAQ versus IMPROVE plots are

Table 3. Location, Elevation (Above Sea Level), and Number of Measurements (N_{meas}) at the Seven AERONET Sites Used for Comparing Monthly AOD Data With CMAQ AOD Columns and MODIS Observations

			N_{meas}			
AERONET Site	Longitude/Latitude, deg	Elevation, m	June	July	August	(Col/Row)
CARTEL	−71.9/45.3	300	22	1	43	130/83
COVE	−75.7/36.9	37	2	6	57	128/55
Howland	−68.7/45.2	100	27	20	27	137/84
MD Science Center	−76.6/39.2	15	1	4	29	125/62
SERC	−76.5/38.8	10	2	5	47	125/61
Wallops	−75.4/37.9	10	32	43	42	128/58
GSFC	−76.8/38.9	87	12	2	42	124/61

located along the gradient contour in the NE area (see Figures 1 and 2). From Figure 2, it is also seen that there is a large difference between the extinctions measured and observed at MACA2 nephelometer located at Mammoth

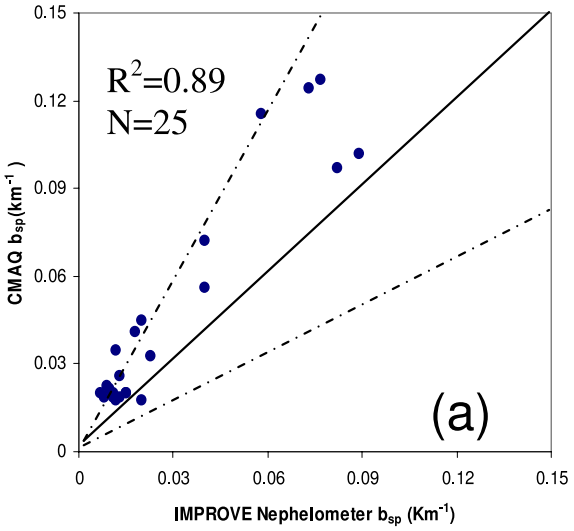

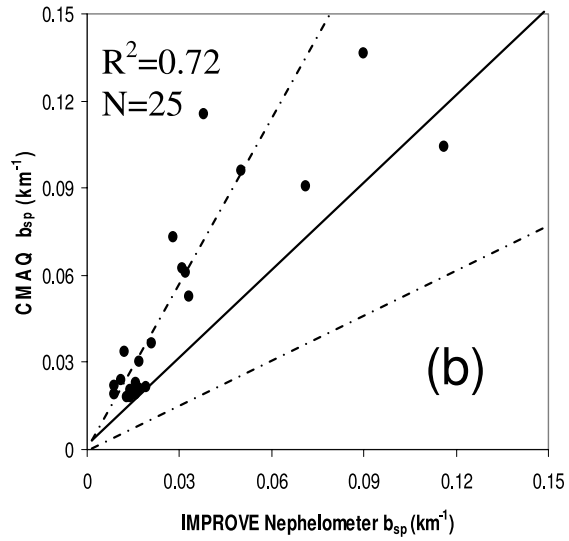

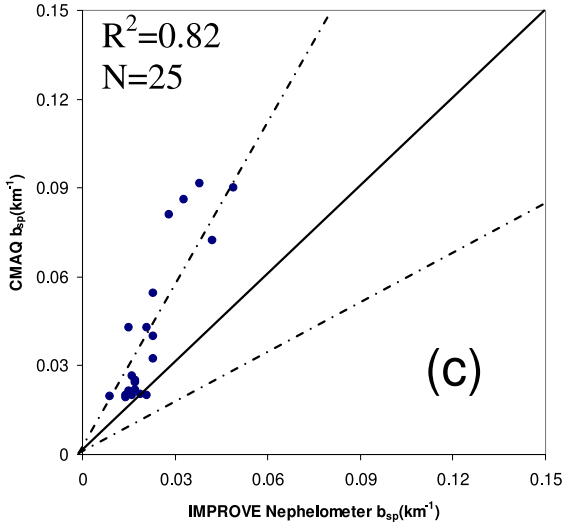

Figure 1. (a) Scatterplot between the CMAQ-derived extinctions (km^{-1}) due to particle scattering only (b_{sp}) obtained using the RM method with the 25 site-month averaged IMPROVE nephelometer b_{sp} data for June 2001. The solid line is 1:1 plot, and the dot-dashed line is the 1:2 and 2:1 plot, respectively. (b) Same as in Figure 1a except for the month of July 2001. (c) Same as in Figure 1a except for the month of August 2001.

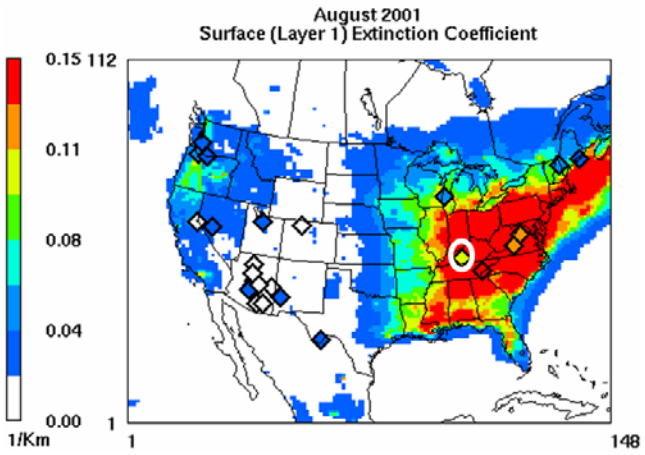

Figure 2. Spatial plot of CMAQ derived monthly average surface extinctions for August 2001 overlaid with the IMPROVE nephelometer average data (in colored diamonds) at respective locations in the continental United States. The nephelometer site MACA2 that has unexplained maximum difference in b_{sp} is located at Mammoth Cave National Park, KY, and is shown inside the white circle.

Cave National Park, KY (shown inside circle in Figure 2). Probability of localized precipitation washout leading to small extinctions registered at MACA2 site is minimum since we did not locate much rainfall activity based on the National Precipitation Analysis rain maps. Comparison of modeled and measured $PM_{2.5}$ concentrations at the IMPROVE sites (not shown), however, indicate a low bias in the model. Thus overprediction of surface extinction at these sites could be related to overestimation of the f(RH) growth factor in the reconstructed mass method used here. The f(RH) is the dimensionless growth factor for converting dry extinctions to ambient values. The f(RH) values are tabulated in a look-up table in increments of 1% RH for a RH range of 0–99%. Thus the f(RH) can be estimated for each model grid cell based on the modeled RH values from the MM5 simulations. Similar adjustment factors are also used in regional haze rule guidance documents that could be viewed at http://vista.cira.colostate.edu/improve/Publications/GuidanceDocs/guidancedocs.htm.

4. Comparison of CMAQ Aerosol Property With Observation Product

4.1. CMAQ AOD With MODIS and AERONET Data

[15] The AOD can be used as an indicator of the atmospheric loading of the fine PM. To explore the relationship between PM loading and AOD, Figure 3 presents scatterplots correlating both the MODIS AOD with MODIS

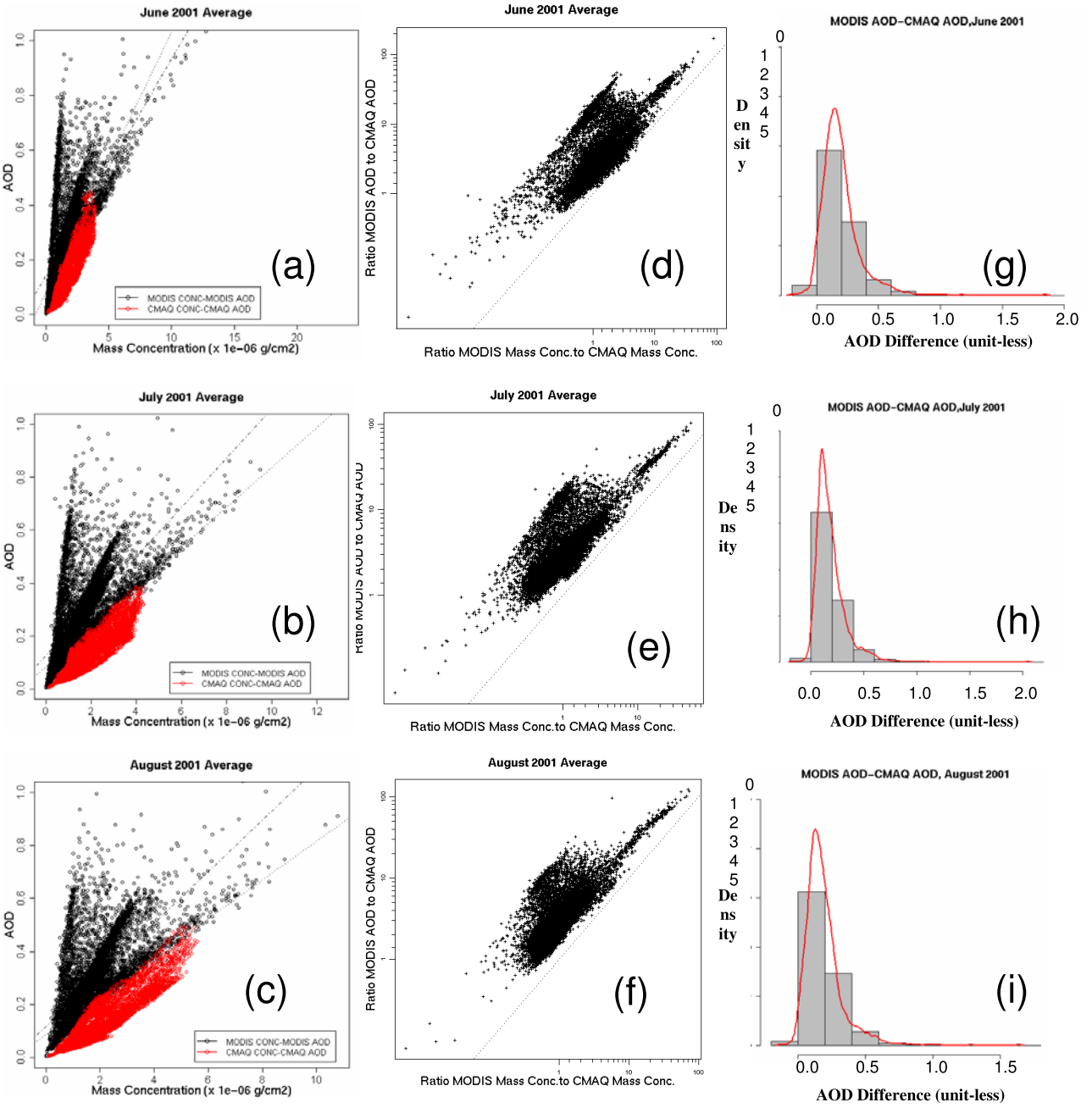

Figure 3. (a–c) Scatter between the monthly average MODIS AOD and monthly average MODIS derived mass concentration (black dots) and CMAQ derived AOD with CMAQ derived average concentration of $PM_{2.5}$ (red dots) with dotted lines showing the linear trend of the data for the June–August months of year 2001. (d–f) Scatterplot of the ratio of MODIS to CMAQ AOD versus ratio of MODIS mass concentration to CMAQ average $PM_{2.5}$ concentration shown in log axis and ordinate. (g–i) Histogram of the monthly average MODIS-CMAQ AOD differences in the continental United States with density plotted with bandwidth = 0.05 (red curve).

mass concentration on a monthly mean basis (shown in Figures 3a–3c). In these comparisons we select a longer (monthly) period in order to ascertain the differences between model and observed data in terms of synoptic-scale activities, and lifetime of few dominant species such as sulfates (few days). The ratios between the CMAQ monthly average AOD and MODIS monthly average AOD are also plotted along with ratio of respective mass concentration in Figures 3d–3f. The MODIS mass concentration is another swath-level product obtained from MOD04_L2 data file whereas CMAQ average concentration (in g cm^{-2}) is computed for $PM_{2.5}$ using the following equation:

$$C_{Avg} = \sum_{i=1}^{N} C_i \, \Delta Z_i \tag{6}$$

where C_i is the $PM_{2.5}$ concentration in μg m^{-3} at the ith layer with a thickness of ΔZ_i in meters. C_i is obtained using

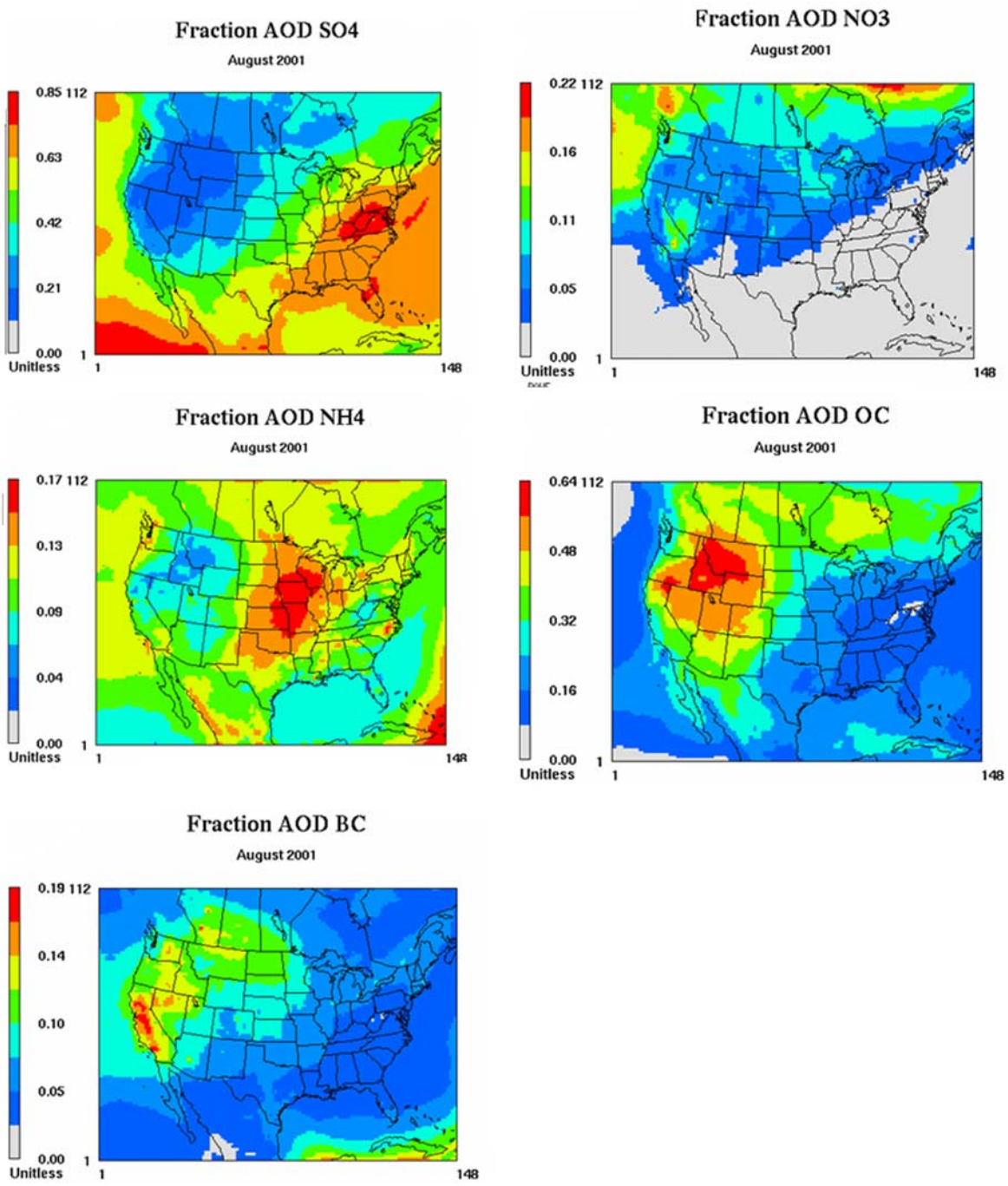

Figure 4. Spatial plot of monthly average fractional AOD columns obtained from five chemical species for August 2001 over the continental United States. Note that the scales are different for each map.

the CMAQ-predicted hourly aerosol species whose description is given by *Binkowski and Roselle* [2003, Table 1]. Clearly, MODIS AOD values are associated with lower mass concentration estimates than that for the CMAQ AOD. A curious feature of these comparisons is that three distinct bands of association between MODIS AOD and mass concentration are evident. This may be an artifact of assumptions intrinsic in the look up tables used in the estimation and retrievals of MODIS AOD and mass concentration. As illustrated in Figures 3d–3f, the MODIS/CMAQ ratios of both AOD and mass concentration are often greater than 1.0 suggesting systematic underprediction of both these quantities in the model relative to the MODIS retrievals.

[16] The histogram and probability density plots for the three months shown in Figures 3g–3i suggest a slight positive skew in each case, the mean of the differences between the monthly average MODIS AOD columns and

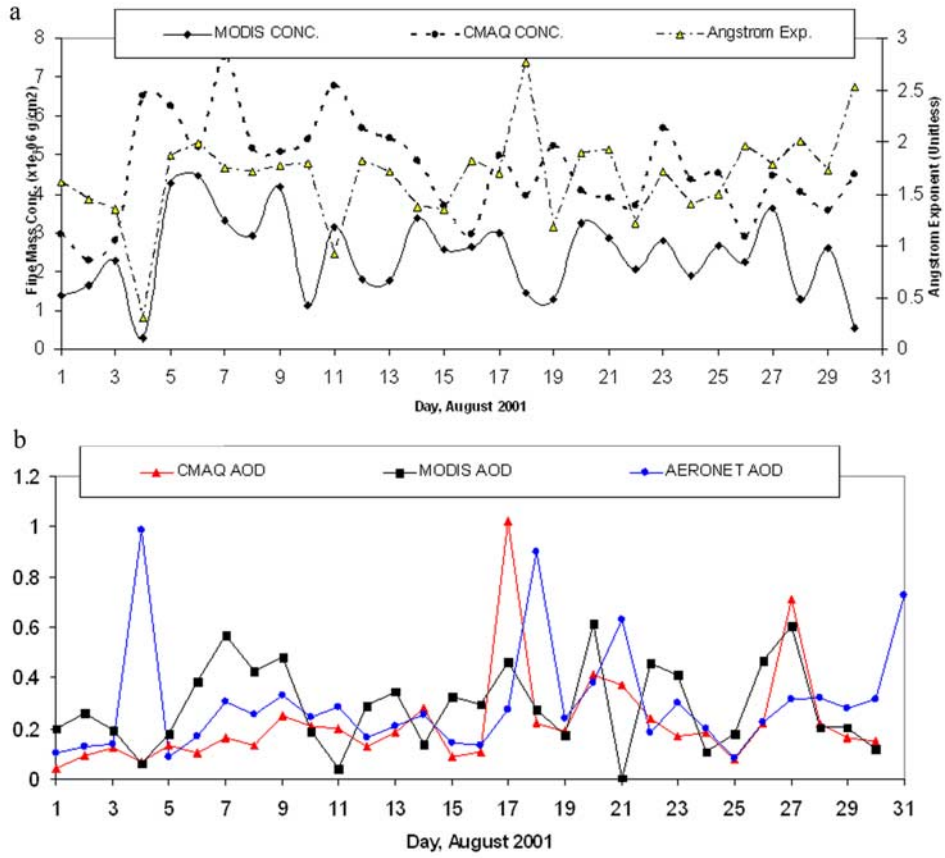

Figure 5. (a) Time series plot of regional daily median values of modeled CMAQ average columnar $PM_{2.5}$ concentration (dashed line) using equation (6) and MODIS (solid line) fine mass concentration data during the period 1–30 August 2001 for the seven northeast U. S. AERONET sites mentioned in Table 3. Time series of MODIS derived Angstrom exponent is also shown in this plot; note its inverse relation with the CMAQ average mass concentration data. (b) Time series of the CMAQ, MODIS and AERONET AOD for the same time period as in Figure 5a.

CMAQ tropospheric AOD is approximately 0.2 for all the three months. Mean difference between respective monthly average columnar mass concentrations data were 0.052, 0.087, and 0.430 ($\times 10^{-6}$ g cm^{-2}) for the months of June, July, and August, respectively.

[17] To examine the relative contribution of the various aerosol chemical constituents to the AOD, Figure 4 presents the spatial plots of monthly mean fractional contributions for SO_4, NO_3, NH_4, Carbon, and coarse-mass during August 2001; from CMAQ results the distribution for June and July 2001 are similar and thus not shown here. It is evident from these spatial distributions that sulfate is a dominant contributor to the AOD in the eastern United States with a relative contribution of about > 60% (over large regions) to the total AOD during summer. Combined OC and BC contribution to the AOD in the eastern United States is ~15%.

[18] Figure 5a presents comparisons of the temporal evolution of regional mean values of the model-predicted tropospheric average $PM_{2.5}$ concentration (using equation (6)) and MODIS mass concentration data along with the MODIS measured regional average Angstrom exponent data for the seven NE U.S. AERONET locations (listed in Table 3) during the month of August 2001. The month of August is selected for this comparison because of completeness in data. In general, the CMAQ and MODIS derived fine PM mass concentration data bear an inverse relation with MODIS Angstrom-exponent time series (see Figure 5a) except for few days during the latter half of the month which could be due to momentary increase in coarse particle concentrations reaching the NE U.S. sites as seen from *Kaufman et al.* [2005, Figure 4] showing the MODIS aerosol monthly composites for year 2001. Figure 5b shows the AOD comparison between AERONET, MODIS and CMAQ. AERONET sensor looking in the bottom-up direction has a better agreement with the CMAQ columnar AOD in the 0.2–0.4 range. Since pollution sources are mostly present within the planetary boundary layer (PBL), hence both CMAQ and AERONET AOD algorithms are explicitly more sensitive to changes in PBL aerosol concentrations than is the MODIS algorithm which relies mostly on the reflectance values from surface and atmosphere for estimating AOD. In an earlier study it was found that the difference in distribution of aerosol properties between the free tropo-

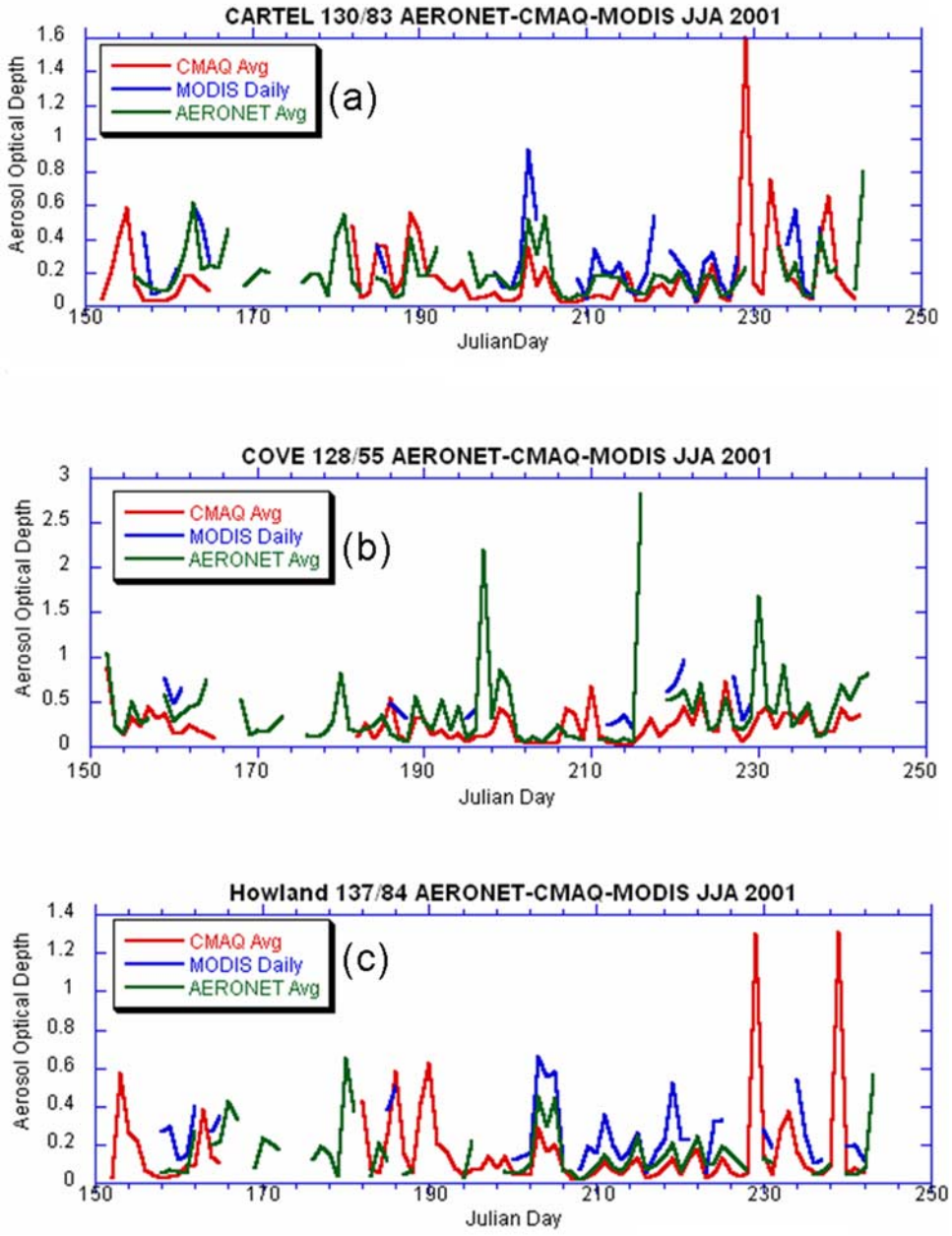

Figure 6. (a–c) CMAQ tropospheric AOD columns shown as time series plot along with AERONET AOD and MODIS AOD columns averaged in daily timescale at the seven AERONET sites in the NE United States. The corresponding CMAQ grid cells where the AERONET sensor is located is mentioned in the main header of each figure. (d–f) CMAQ tropospheric AOD columns shown as time series plot along with AERONET AOD and MODIS AOD columns averaged in daily timescale at the seven AERONET sites in the NE United States. The corresponding CMAQ grid cells where the AERONET sensor is located is mentioned in the main header of each figure. (g) CMAQ tropospheric AOD columns shown as time series plot along with AERONET AOD and MODIS AOD columns averaged in daily timescale at the seven AERONET sites in the NE United States. The corresponding CMAQ grid cells where the AERONET sensor is located is mentioned in the main header.

sphere and the PBL are statistically significant at the 3% level or better [*Sheridan and Ogren*, 1999]; hence we think that AERONET and CMAQ will be more sensitive to PBL changes in aerosol properties than for the free tropospheric levels.

[19] A comparison of model predictions (surface) to observations (Table 1) shows a very reasonable performance for seasonally averaged SO_4^{2-} and less prediction performance of seasonally averaged NO_3^- and carbonaceous aerosols. The present study is a demonstration that sulfate

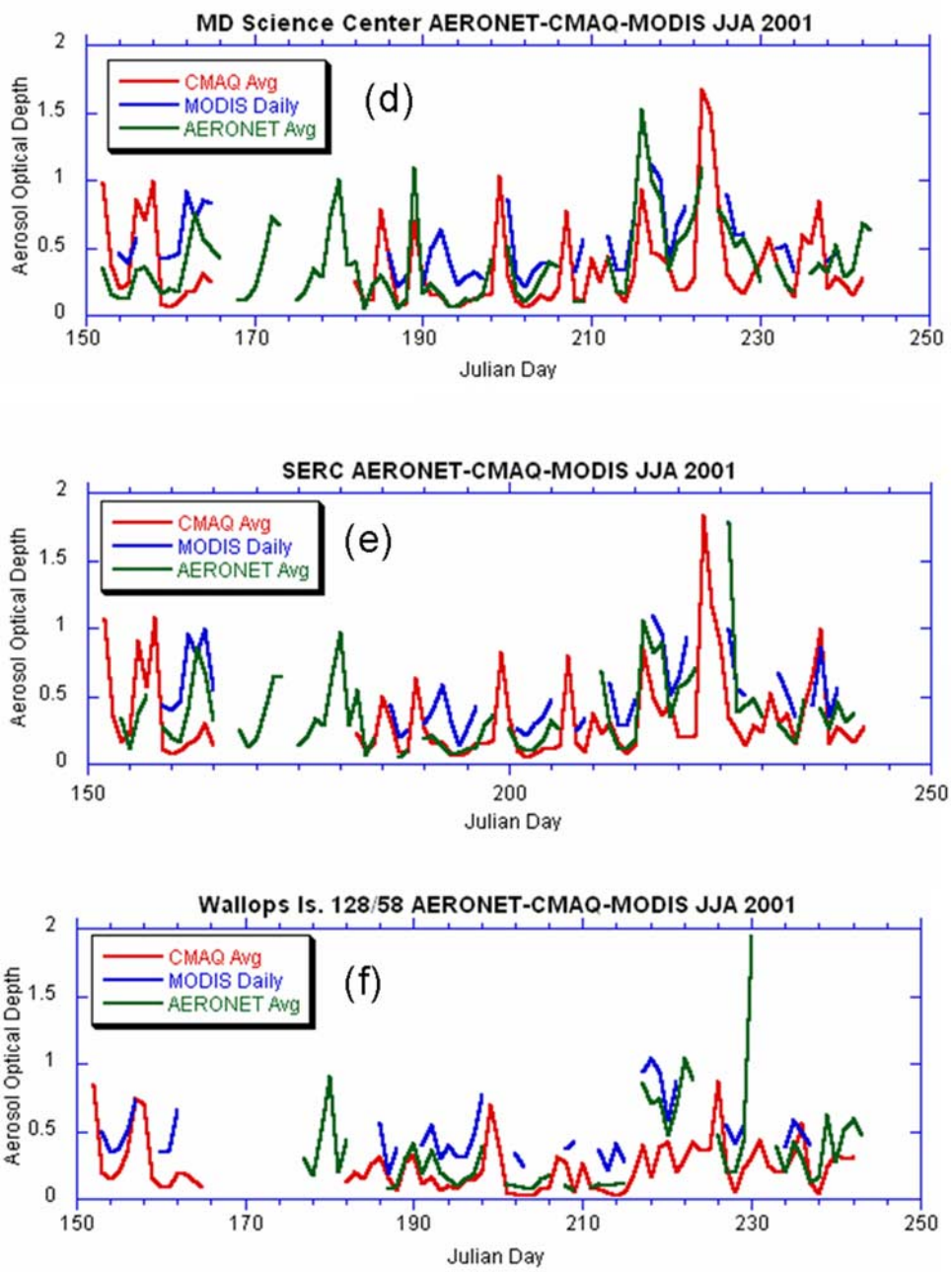

Figure 6. (continued)

dominates aerosol optical depths in polluted regions in the northeast United States provides encouragement that the total AOD from CMAQ could agree well with satellite derived AOD however, these prediction errors in the OC and BC will impact the resulting AOD to some degree. We find contributions from BC and OC in the mid-Atlantic region do not appear to be more than 15% of the columnar AOD.

[20] In order to quantitatively assess the model's ability to capture the day-to-day variations in simulated AOD, Figure 6 presents comparisons of temporal variations in the predicted AOD with those inferred from MODIS and AERONET at the same seven northeastern U.S. sites (see Table 3). From Figures 6a–6g it is evident that there is a moderate agreement between the CMAQ AOD and AERONET AOD. The relative sparsity in MODIS data at these sites during this period is due to cloudiness. Temporal trend between the predicted and observed AOD is similar. In order to assess CMAQ's ability to capture the regional patterns in aerosol loading and its temporal variability, comparison of regional distributions of AOD derived from the model and MODIS are presented in Figures 7 and 8 for the 16–19 July and 12–15 August 2001 periods, respectively. From Figures 7 and 8, we can infer that the AOD distributions from CMAQ show some degree of positive correspondence with the MODIS spatial AOD patterns.

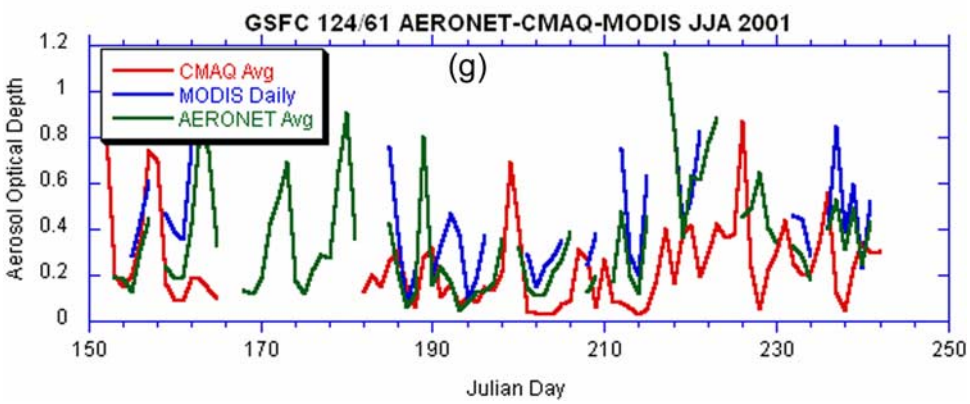

Figure 6. (continued)

Some distinct AOD patterns from the model are noticeable that represent transport of PM mass across the entire eastern region. For the purpose of verifying the MODIS missing data due to presence of clouds we have plotted the Geostationary Operational Environmental Satellite (GOES 8) 1800 UTC visible images along with the MODIS and CMAQ daily AOD data (see Figure 7, right side).

[21] It is interesting to note from Figure 7 that high CMAQ AOD field is concomitant with cloud cover (compare left CMAQ AOD plots with GOES 8 derived cloud images shown in Figure 7, right side). We have already pointed out that sulfates are a major contributor to AOD and here we are also seeing a strong CMAQ AOD contribution over the cloudy regions. We find a strong spatial correspondence between daily CMAQ AOD, GOES derived cloud field at 1800 UTC, and the daily average sulfate concentration derived using equation (6). Using a sulfate mass prediction model *Kiehl et al.* [2000] found that hygroscopic growth effects produce prominent scattering at higher relative humidity (>90%) resulting in strong direct effect (cooling) and enhanced cloud optical thickness. Hence we attribute enhanced CMAQ AOD over the cloudy region due to higher extinctions resulting from in-cloud sulfate production and higher relative humidity in the vicinity of clouds. In addition, we have found that the MODIS-CMAQ differences in AOD increased with increase in $PM_{2.5}$ loadings at the surface (measured by the IMPROVE sensor) and shows a maximum difference at a surface $PM_{2.5}$ concentration $\sim$10–12 μg m^{-3}. An important point could be made on the basis of this study, i.e., assuming no gross model misrepresentation satellite derived AOD can miss some of the highest daily AOD values because they can occur in the presence of cloud whereas the model could easily predict in-cloud sulfate contributions to AOD.

[22] Since the MODIS algorithm for reflectance based AOD retrieval involves a very detailed procedure for the selection of an aerosol model that describes its size distribution and assigns values of refractive index and single scattering albedo based on the selected model, we also consider if the variation of the gross indicator of aerosol size distribution (Angstrom exponent) from the satellite data has any relation with the aerosol mass concentration and AOD obtained directly from the model.

4.2. MODIS Angstrom Exponent and CMAQ Mass Concentration Data

[23] The spectral dependence of aerosol optical depth is represented by the Angstrom exponent [*Angstrom*, 1964; *Eck et al.*, 1999, *Reid et al.*, 1999; *Pinker et al.*, 2004]. This is mathematically represented as:

$$AOD(\lambda) = K\lambda^{-a} \tag{7}$$

where AOD(λ) is the spectral aerosol optical depth at wavelength λ (in μm), K is the Angstrom turbidity coefficient (which equals 1 at λ = 1 μm), and α is the Angstrom exponent. This parameter, derived from Sun photometry in the 437–669 nm wavelength interval is found to be well correlated with particle size [*Reid et al.*, 1999]. The Angstrom exponent is an indicator of particle size since it is related to the power law size distribution [*Junge*, 1955] as mentioned in *Eck et al.* [1999] and *Seinfeld and Pandis* [1998]. The typical values of α range from >2.0 for fresh smoke particles dominated by accumulation mode aerosols to nearly zero for high AOD dominated by coarse mode aerosols as mentioned by *Eck et al.* [1999] and *Saha and Moorthy* [2005]. *Eck et al.* [2001] have shown that the monthly average Angstrom exponent at a station in Maldives Island (Indian Ocean) during the Indian Ocean Experiment (INDOEX) shows a pattern that matches with the shift in air mass trajectories from cities to desert and change in α values from 1.2 to 0.45 during the period April–June 1998.

Figure 7. Spatial plots for daily averaged column AOD from CMAQ (left plot in each row) and MODIS data (middle plot in each row) for eventful periods on 16, 17, 18, and 19 July 2001 and during another eventful period 12–15 August 2001. Note missing data from MODIS sets due to presence of cloud. The right plot in each row has the 1800 UTC daily retrospective GOES 8 visible images showing presence of clouds in the eastern United States. Note correspondence between strong CMAQ AOD (left plots) with cloudy fields from GOES 8 (right plots).

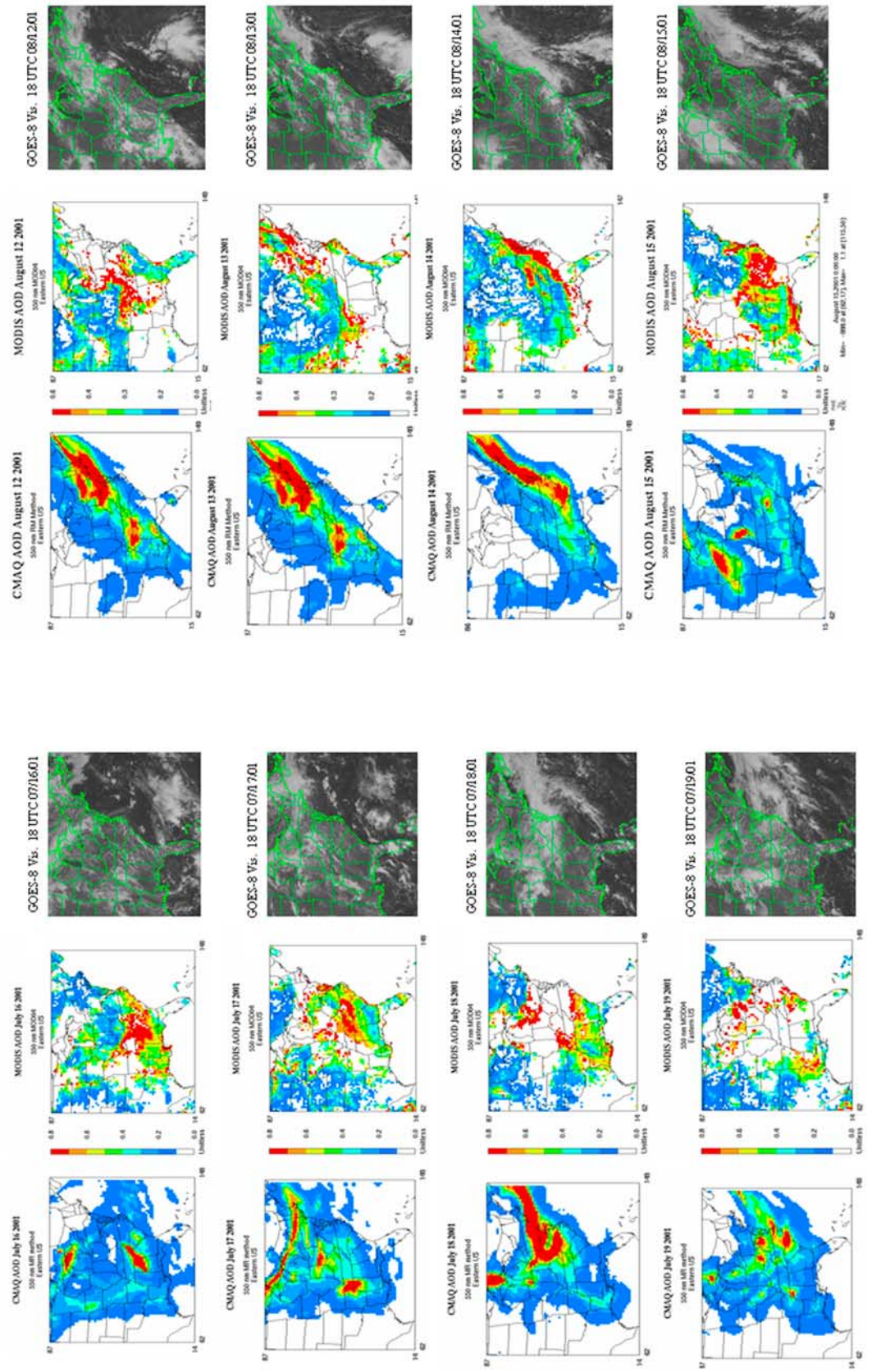
GOES-8 Vis. 18 UTC 08/12/01
GOES-8 Vis. 18 UTC 08/13/01
GOES-8 Vis. 18 UTC 08/14/01
GOES-8 Vis. 18 UTC 08/15/01
MODIS AOD August 12 2001
MODIS AOD August 13 2001
MODIS AOD August 14 2001
MODIS AOD August 15 2001
CMAQ AOD August 12 2001
CMAQ AOD August 13 2001
CMAQ AOD August 14 2001
CMAQ AOD August 15 2001
GOES-8 Vis. 18 UTC 07/16/01
GOES-8 Vis. 18 UTC 07/17/01
GOES-8 Vis. 18 UTC 07/18/01
GOES-8 Vis. 18 UTC 07/19/01
MODIS AOD July 16 2001
MODIS AOD July 17 2001
MODIS AOD July 18 2001
MODIS AOD July 19 2001
CMAQ AOD July 16 2001
CMAQ AOD July 17 2001
CMAQ AOD July 18 2001
CMAQ AOD July 19 2001

Figure 7

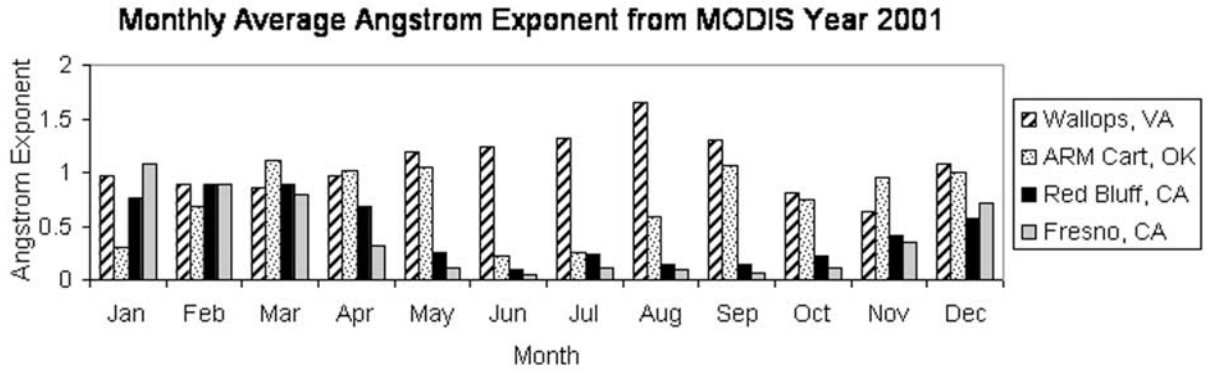

Figure 8. Monthly mean variation of MODIS observed Angstrom exponent as observed at four AERONET station locations in the continental United States.

[24] The MODIS Angstrom exponent swath product in MOD04_L2 data set has been used in this analysis. We examine monthly mean values at 4 locations each corresponding to an AERONET site. These sites were chosen so as to cover the entire east-west span of the continental United States. Two California sites are chosen for the purpose of redundancy in our analysis since the MODIS algorithm poorly represents aerosol properties in the western United States. Wallops Island site in Virginia is used to represent the eastern U.S. conditions, the Department of Energy's Atmospheric Radiation Monitoring Cloud and Radiation Testbed (DOE ARM CART) site in the Southern Great Plains (north central Oklahoma) represents the central United States, and Red Bluff, and Fresno sites both in California represent the western United States. The seasonal variation of Angstrom exponent for the year 2001 at each site-month is shown using bar plots (see Figure 8). It is apparent from Figure 8 that there are smaller particle sizes dominant over the Wallops site during the June–August period compared with the DOE ARM Cart site in the central United States and the western sites. In general the α values observed in the visible spectrum are much higher at the eastern site (1.25 to 1.6). Figure 9a shows the bar plot comparing the site-season (June–August) averaged CMAQ mass concentration data with those obtained from MODIS observations over the four selected sites. From Figure 9a it is apparent that the CMAQ-MODIS difference is higher at the Southern Great Plains (ARM CART) site as compared with other sites in the east and western part of the United States. Figure 9b shows the CMAQ and MODIS seasonal mean AOD over the four selected sites along with the average value of the Angstrom exponent. These results suggest that coarse particle loadings dominate in the western part of the United States ($\alpha \sim 0.2$) whereas the eastern part of the United States has more local pollution episodes resulting in higher fine mass concentration which result in α values in the range 1.2–1.4. CMAQ does not perform very well in the western part since there is at present a major deficiency in fugitive dust emissions input information to CMAQ. There are also other challenges in the western part of the United States in addition to orographic effects that cannot be captured well at the present 36-km resolution along with a few other uncertainties.

5. Summary

[25] To consider satellite-observed AOD as an additional data source for evaluating $PM_{2.5}$ predictions from atmospheric chemistry transport models to augment analysis with routine surface observations, the Terra/MODIS AOD standard swath-level product has been compared with CMAQ model derived AOD computed using the *Malm et al.* [1994] semiempirical method. In order to provide a basis for these comparisons we have also compared model results with measurements from AERONET and IMPROVE sites in the eastern United States. The focus is primarily on the eastern United States because MODIS products have better confidence in this region that has abundant vegetation cover thus providing excellent dark targets leading to a better performance of the MODIS AOD retrieval technique.

[26] CMAQ-derived surface extinction based on the reconstructed mass (RM) method [*Malm et al.*, 1994] compare well with the IMPROVE nephelometer particle extinction data. This provides confidence in the use of the RM method to estimate 3-D extinction fields needed to estimate the CMAQ AOD. The relationship between CMAQ monthly mean mass concentration and tropospheric AOD column are found to be scattered in ranges much lower than that obtained between the monthly mean MODIS mass concentration and MODIS AOD column data. Hence we infer that both modeled AOD and average tropospheric mass concentrations are underestimated relative to the MODIS retrievals.

[27] This is consistently observed for all the three summer months examined here. The mean difference between the MODIS columnar AOD and CMAQ tropospheric AOD data for the June-August 2001 period is found to be 0.2. Sulfate is found to contribute to >60% of AOD over the large portions of the eastern United States ratio of MODIS to CMAQ tropospheric AOD is often a factor of 1 to 10 higher than the ratio of MODIS to CMAQ column average $PM_{2.5}$ mass concentrations. This implies a systematic

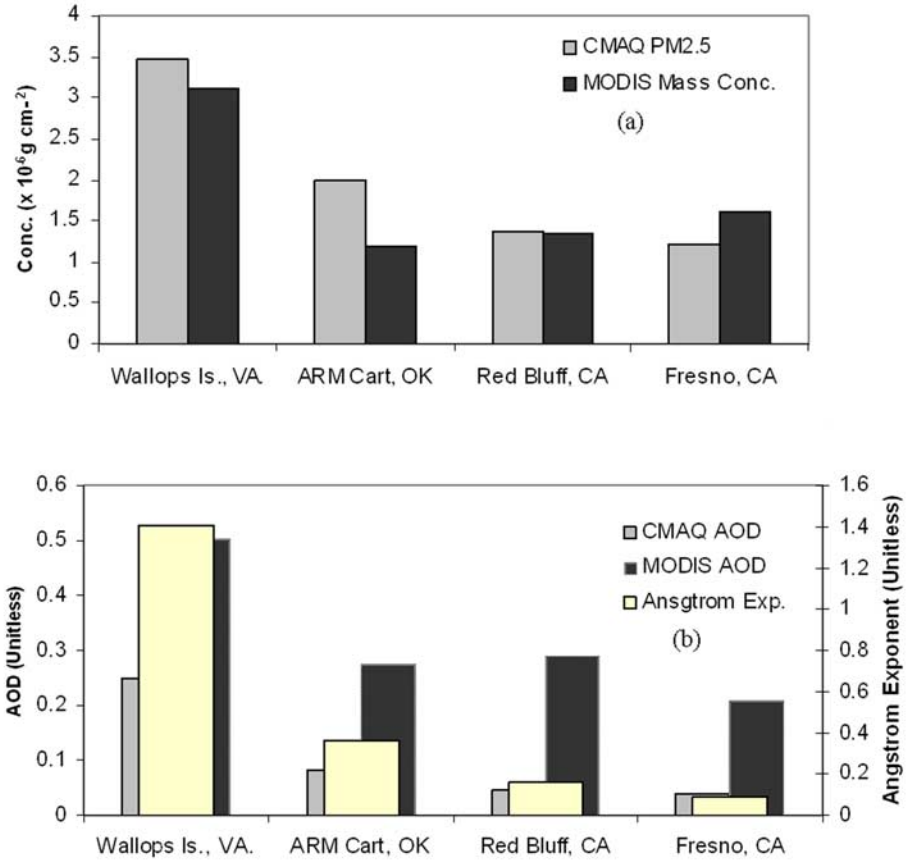

Figure 9. (a) CMAQ average (June–August 2001) $PM_{2.5}$ concentration data and MODIS derived mass concentration data for the Wallops Island, VA; DOE ARM CART site, OK; Red Bluff, CA; and Fresno, CA, sites, respectively. (b) CMAQ and MODIS AOD average data for the same four sites as mentioned for Figure 9a along with the MODIS estimated Angstrom exponent for the four sites.

difference in the relationship between mass loading and AOD represented in the model from that in the MODIS retrieval algorithm. There are several possible reasons for these discrepancies: (1) assumptions on aerosol composition and size distribution in the MODIS retrieval algorithm, (2) presence of elevated aerosol layers from the long-range transport that are detected by the MODIS but not represented in the model, (3) inherent differences due to subgrid-scale variability and temporal resolution in the model neglecting the effects of smoothing due to temporal averaging, and (4) possible effects associated with lateral boundary condition specifications especially for the aloft model layers. It could be pointed out that CMAQ model representation of elevated aerosol layers could be improved by setting up boundary conditions using more recent active sensing of aerosol profile measurements made from instruments from the recently launched Cloud-Aerosol Lidar and Infrared Pathfinder Satellite Observation (CALIPSO) mission and also using the output from global air quality models; the applicability of these techniques is currently under investigation.

[28] Comparisons of daily spatial AOD distributions predicted by CMAQ with corresponding MODIS distributions (Figure 7) show that the model captures the regional-scale distributions as well as the day-to-day variability arising from mesoscale/synoptic activity. Often regions with high model-predicted AOD were found to correspond with regions of observed widespread cloudiness, suggesting the role of in-cloud SO_4^{2-} formation on total column AOD. It should be noted that modeled AOD in these regions cannot be verified against MODIS because of cloud contamination in the satellite derived values. Temporal variations in the daily average CMAQ AOD at a variety of AERONET sites were found to be consistent with those inferred from both the ground based AERONET as well as the space-based MODIS data. Spectral variation in AOD as parameterized by the Angstrom exponent (α) also exhibited intraseasonal variability with a high value of α for the eastern U.S. sites, signifying more pollution associated with fine particles in the eastern states than in the western sites (dominated by more arid regions) with enhanced coarse-mode suspended particles during the summer period. Such a seasonal trend in the Angstrom exponent monthly mean values suggests there is a wide range of variability in aerosol size distribution as observed by the satellite, signifying summertime small particle sizes in the eastern part of the United States and relatively larger particle size in the western part of the United States CMAQ-predicted average mass ($PM_{2.5}$) con-

centrations also similarly cause high extinctions resulting in high AOD values over the eastern AERONET sites. The discrepancy between the modeled and observed AOD is greater when examined zonally as we go from the eastern to the western parts of the continental United States during the June–August period (see Figure 9b). This also corresponds with a decrease in CMAQ-predicted average sulfate concentration profile to a greater extent, than a shift in the mass concentration profile as we go from east to west.

[29] The upward looking AERONET and downward looking MODIS sensors provide good quality data for a thorough evaluation of the CMAQ-predicted aerosol properties. These remotely sensed data are used for the first time for CMAQ evaluation in this study. The key results of our analysis can be summarized as (1) CMAQ surface extinction due to particle scattering at 550 nm wavelength capture the spatial gradients in the NE United States; (2) synoptic-scale variability observed in the MODIS AOD are captured well by CMAQ; (3) regions of high predicted AOD show strong spatial correspondence with observed cloudiness signifying occurrence of enhanced optical extinction due to in-cloud sulfate production in regions of higher relative humidity; (4) CMAQ AOD values are found to be lower than the MODIS AOD for the same $PM_{2.5}$ concentrations, and MODIS-CMAQ differences in AOD increase with increase in surface $PM_{2.5}$; and (5) MODIS AOD as a function of mass concentration shows a trimodal pattern. We conjecture that such a pattern in AOD distribution with respect to mass concentration occurs because of assumptions in the look-up tables being used in MODIS retrievals of AOD and mass concentration. A proper selection of the look up tables may result in harmonization of MODIS AOD product with those estimated using CMAQ-predicted aerosol concentration data. Using observed and modeled extinctions data some key information about CMAQ's performance for prediction of surface $PM_{2.5}$ contributions to AOD have been identified; however, further testing and investigation is warranted before using satellite AOD on an operational basis for model evaluation.

[30] **Acknowledgments.** The authors wish to thank Lucille Bender of the Computer Sciences Corporation and Alfreida Torian of Atmospheric Sciences Modeling Division for their help with the modeling results and obtaining data. We wish to thank Lawrence Friedl of NASA headquarters for his help in providing the MODIS quality-controlled data sets used in this study; Brent Holben of NASA GSFC for his efforts in maintaining COVE, Howland, Maryland Science Center, Philadelphia, SERC, Wallops, and Goddard Space Flight Center (GSFC) AERONET sites; and N. T. O'Neill of Université de Sherbrooke, Quebec, Canada, for maintaining the CARTEL AERONET site whose data have been widely used in this paper. We also wish to thank Shawn McClure of the CIRA (Colorado State University) and Joe Adlhoch of Air Resource Specialists, Inc., Fort Collins, Colorado, for their help in providing the IMPROVE nephelometer data and explaining the details about the IMPROVE aerosol (raw) program from which data have been obtained. We also thank David Mobley and Tanya Otte of the Atmospheric Modeling Division for their valuable suggestions. The research presented here was performed under the memorandum of understanding between the U.S. Environmental Protection Agency (EPA) and NOAA and under agreement DW13921548. This work constitutes a contribution to the NOAA Air Quality Program. Although it has been reviewed by EPA and NOAA and approved for publication, it does not necessarily reflect their policies or views.

References

Al-Saadi, J., et al. (2005), Improving national air quality forecasts with satellite aerosol observations, *Bull. Am. Meteorol. Soc.*, *86*(9), 1–13.

Angstrom, A. (1964), The parameters of atmospheric turbidity, *Tellus*, *16*, 64–75.

Appel, W., A. B. Gilliland, and B. Eder (2005), An operational evaluation of the 2005 release of Models-3 CMAQ Version 4.5, paper presented at 4th Annual Community Modeling and Analysis System (CMAS) Models-3 Users' Conference, Chapel Hill, N. C., 26–28 Sept. (Available at http://www.cmascenter.org/help/model_docs/cmaq/4.5/Model_Performance_Evaluation.pdf)

Bey, I., D. J. Jacob, R. M. Yantosca, J. A. Logan, B. D. Field, A. M. Fiore, Q. Li, H. Y. Liu, L. J. Mickley, and M. G. Schultz (2001), Global modeling of tropospheric chemistry with assimilated meteorology: Model description and evaluation, *J. Geophys. Res.*, *106*, 23,073–23,096.

Binkowski, F. S., and S. J. Roselle (2003), Models-3 Community Multiscale Air Quality (CMAQ) model aerosol component: 1. Model description, *J. Geophys. Res.*, *108*(D6), 4183, doi:10.1029/2001JD001409.

Byun, D. W., and J. K. S. Ching (1999), Science algorithms of the EPA Models-3 Community Multiscale Air Quality (CMAQ) modeling system, *Rep. EPA/600/R-99/030*, U.S. Environ. Prot. Agency, Washington, D. C.

Byun, D. W., and K. L. Schere (2006), Review of the governing equations, computational algorithms, and other components of the Models-3 Community Multiscale Air Quality (CMAQ) modeling system, *Appl. Mech. Rev.*, *59*, 51–77.

Dudhia, J. (1989), Numerical study of convection observed during the winter monsoon experiment using a mesoscale two-dimensional model, *J. Atmos. Sci.*, *46*, 3077–3107.

Eck, T. F., B. N. Holben, J. S. Reid, O. Dubovik, A. Smirnov, N. T. O'Neill, I. Slutsker, and S. Kinne (1999), Wavelength dependence of the optical depth of biomass burning, urban, and desert dust aerosols, *J. Geophys. Res.*, *104*, 31,333–31,349.

Eck, T. F., B. N. Holben, O. Dubovik, A. Smirnov, I. Slutsker, J. M. Lobert, and V. Ramanathan (2001), Column-integrated aerosol optical properties over the Maldives during the northeast monsoon for 1998–2000, *J. Geophys. Res.*, *106*, 28,555–28,566.

Gery, M. W., G. Z. Whitten, J. P. Killus, and M. C. Dodge (1989), A photochemical mechanism for urban and regional scale computer modeling, *J. Geophys. Res.*, *94*, 12,925–12,956.

Gilliam, R. C., C. Hogrefe, and S. T. Rao (2006), New methods for evaluating meteorological models used in air quality applications, *Atmos. Environ.*, *40*, 5073–5086.

Gilliland, A. B., S. R. Roselle, R. Pinder, and R. L. Dennis (2006), Seasonal NH_3 emissions for an annual 2001 CMAQ simulation: Inverse model estimation and evaluation, *Atmos. Environ.*, *40*, 4986–4998.

Grell, G., A. J. Dudhia, and D. Stauffer (1994), A description of the fifth-generation Penn State/NCAR mesoscale model (MM5), *NCAR Tech. Note TN-398+STR*, 138 pp., Natl. Cent. for Atmos. Res., Boulder, Colo.

Hauser, A., D. Oesch, and N. Foppa (2005), Aerosol optical depth over land: Comparing AERONET, AVHRR, and MODIS, *Geophys. Res. Lett.*, *32*, L17816, doi:10.1029/2005GL023579.

Holben, B. N., et al. (1998), AERONET—A federated instrument network for aerosol characterization, *Remote Sens. Environ.*, *66*, 1–16.

Junge, C. E. (1955), The size distribution and aging of natural aerosols as determined from electrical and optical data on the atmosphere, *J. Meteorol.*, *12*, 13–25.

Kain, J. S. (2004), The Kain-Fritcsh convective parameterization: An update, *J. Appl. Meteorol.*, *43*, 170–181.

Kaufman, Y. J., and D. Tanré (1998), Algorithm for remote sensing of tropospheric aerosol from MODIS, Product ID: MOD04, report, 84 pp., NASA Goddard Space Flight Cent., Greenbelt, Md.

Kaufman, Y. J., D. Tanré, L. A. Remer, E. F. Vermote, D. A. Chu, and B. N. Holben (1997), Operational remote sensing of the tropospheric aerosol over the land from EOD-MODIS, *J. Geophys. Res.*, *102*, 17,051–17,061.

Kaufman, Y. J., N. Gobron, B. Pinty, J. L. Widlowski, and M. M. Verstraete (2002), Relationship between surface reflectance in the visible and mid-IR used in MODIS aerosol algorithm—Theory, *Geophys. Res. Lett.*, *29*(23), 2116, doi:10.1029/2001GL014492.

Kaufman, Y. J., I. Koren, L. A. Remer, D. Tanre, P. Ginoux, and S. Fan (2005), Dust transport and deposition observed from the Terra-Moderate Resolution Imaging Spectroradiometer (MODIS) spacecraft over the Atlantic Ocean, *J. Geophys. Res.*, *110*, D10S12, doi:10.1029/2003JD004436.

Kiehl, J. T., T. L. Schneider, P. J. Rasch, and M. C. Barth (2000), Radiative forcing due to sulfate aerosols from simulations with the National Center for Atmospheric Research Community Climate Model, version 3, *J. Geophys. Res.*, *105*, 1441–1457.

King, M. D., and D. M. Byrne (1976), A method for inferring total ozone content from spectral variation of total optical depth obtained with a solar radiometer, *J. Atmos. Sci.*, *33*, 2242–2251.

Levy, R. C., L. A. Remer, J. V. Martins, and Y. J. Kaufman (2005), Evaluation of the MODIS aerosol retrievals over ocean and land during CLAMS, *J. Atmos. Sci.*, *62*, 974–992.

Liu, Y., R. J. Park, D. J. Jacob, L. Qinbin, V. Kilaru, and J. A. Sarnat (2004), Mapping annual mean ground-level $PM_{2.5}$ concentrations using Multiangle Imaging Spectroradiometer aerosol optical thickness over the contiguous United States, *J. Geophys. Res.*, *109*, D22206, doi:10.1029/2004JD005025.

Malm, W. C., J. F. Sisler, D. Huffman, R. A. Eldred, and T. A. Cahill (1994), Spatial and seasonal trends in particle concentration and optical extinction in the United States, *J. Geophys. Res.*, *99*, 1347–1370.

Malm, W. C., B. A. Schichtel, M. L. Pitchford, L. L. Ashbaugh, and R. A. Eldred (2004), Spatial and monthly trends in speciated fine particle concentration in the United States, *J. Geophys. Res.*, *109*, D03306, doi:10.1029/2003JD003739.

Mlawer, E. J., S. J. Taubman, P. D. Brown, M. J. Iacono, and S. A. Clough (1997), Radiative transfer for inhomogeneous atmospheres: RRTM, a validated correlated-k model for the longwave, *J. Geophys. Res.*, *102*, 16,663–16,682.

Nenes, A., S. N. Pandis, and C. Pilinis (1998), ISORROPIA: A new thermodynamic equilibrium model for multiphase multicomponent inorganic aerosols, *Aquat. Geochem.*, *4*, 123–152.

Penner, J. E., H. Eddleman, and T. Novakov (1994), Global emissions and models of photochemically active compounds, in *Global Atmospheric-Biospheric Chemistry*, edited by R. Prinn, pp. 223–248, Plenum, New York.

Pinder, R. W., R. Strated, C. I. Davidson, and P. J. Adams (2004), A temporally and spatially resolved ammonia emission inventory for dairy cows in the United States, *Atmos. Environ.*, *38*, 3747–3756.

Pinker, R. T., G. Pandithurai, B. N. Holben, T. O. Keefer, and D. Goodrich (2004), Aerosol radiative properties in the semiarid western United States, *Atmos. Res.*, *71*, 243–252.

Pleim, J. E., and J. Chang (1992), A non-local closure method for vertical mixing in the convective boundary layer, *Atmos. Environ.*, *26*, 965–981.

Pleim, J. E., and A. Xiu (2003), Development of a land surface model, Part II: Data assimilation, *J. Appl. Meteorol.*, *42*, 1811–1822.

Reid, J. S., T. F. Eck, S. A. Christopher, P. V. Hobbs, and B. N. Holben (1999), Use of the Angstrom exponent to estimate the variability of optical and physical properties of aging smoke particles in Brazil, *J. Geophys. Res.*, *104*, 27,473–27,489.

Reisner, J., R. M. Rasmussen, and R. T. Bruintjes (1998), Explicit forecasting of supercooled liquid water in winter storms using the MM5 mesoscale model, *Q. J. R. Meteorol. Soc.*, *124*, 1071–1107.

Remer, L. A., et al. (2005), The MODIS aerosol algorithm, products, and validation, *J. Atmos. Sci.*, *62*, 947–973.

Saha, A., and K. K. Moorthy (2005), Interannual variations of aerosol optical depth over coastal India: Relation to synoptic meteorology, *J. Appl. Meteorol.*, *44*, 1066–1077.

Seinfeld, J. H., and S. N. Pandis (1998), *Atmospheric Chemistry and Physics*, 1326 pp., John Wiley, Hoboken, N. J.

Sheridan, P. J., and J. A. Ogren (1999), Observations of the vertical and regional variability of aerosol optical properties over the central and eastern North America, *J. Geophys. Res.*, *104*, 16,793–16,805.

U.S. Environmental Protection Agency (2003), User's guide to MOBILE6.1 and MOBILE6.2, *Rep. EPA420-R-03-010*, 262 pp., Assess. and Stand. Div., Off. of Transp. and Air Quality, Washington, D. C.

Xiu, A., and J. E. Pleim (2001), Development of a land surface model. Part I: Application in a mesoscale meteorological model, *J. Appl. Meteorol.*, *40*, 192–209.

A. B. Gilliland, S. C. Howard, and R. Mathur, Atmospheric Sciences Division, Air Resources Laboratory, NOAA, Mail Code E243-03, 109 T. W. Alexander Drive, Research Triangle Park, NC 27711-0001, USA.

B. Roy, National Exposure Research Laboratory, U.S. Environmental Protection Agency, Mail Code E243-01, 109 T. W. Alexander Drive, Research Triangle Park, NC 27711-0001, USA. (roy.dev@epa.gov)